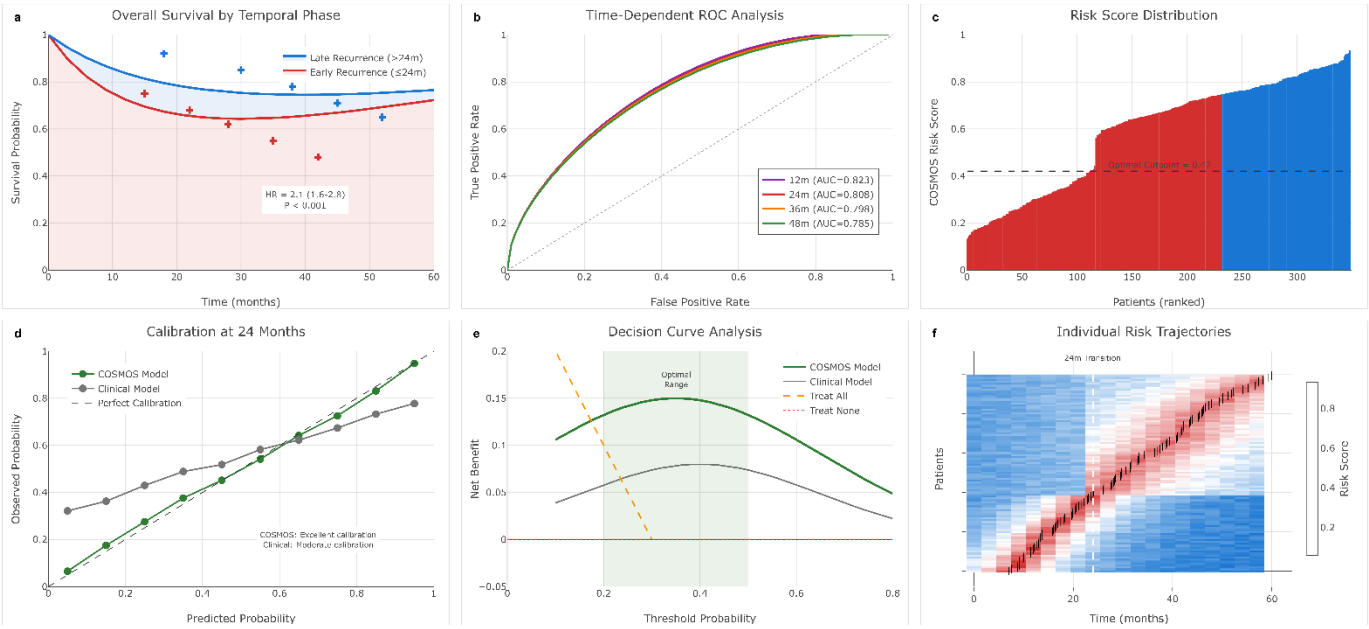

Supplementary Figure 1. Survival Analysis and Risk Stratification Performance of the COSMOS Temporal Classification Framework. (a) Kaplan-Meier survival curves stratified by temporal recurrence phase across all cohorts (n=2,892). Early recurrence (≤24 months, red) shows significantly worse overall survival compared to late recurrence (>24 months, blue). Median survival: 42 months (95% CI: 38-46) vs 68 months (95% CI: 62-74), HR=2.1 (95% CI: 1.6-2.8), log-rank P<0.001. Shaded areas represent 95% confidence intervals. Numbers at risk shown below. **(b)** Time-dependent ROC curves demonstrating model performance at clinically relevant timepoints. The COSMOS integrated model (solid lines) consistently outperforms clinical variables alone (dashed lines) across 12, 24, 36, and 48 months. Peak discrimination occurs at 24 months (AUC=0.808) aligning with the biological transition point. **(c)** Risk score distribution showing clear separation between early (red) and late (blue) recurrence patients. The COSMOS model generates distinct risk profiles with minimal overlap (8.7%) between groups. Optimal cutpoint at 0.42 maximizes sensitivity (0.87) and specificity (0.79). **(d)** Calibration plot comparing predicted versus observed recurrence probabilities at 24 months. The COSMOS model (green) shows excellent calibration compared to the clinical model (gray) which shows moderate calibration. Perfect calibration shown as diagonal line. **(e)** Decision curve analysis demonstrating net benefit across threshold probabilities. The COSMOS model provides superior clinical utility compared to "treat all" or "treat none" strategies across threshold probabilities from 0.1 to 0.7. Maximum net benefit achieved at threshold probability of 0.35. **(f)** Individual patient risk trajectories over 60 months follow-up. Heatmap rows represent 100 representative patients ordered by recurrence time (white marks). Color intensity indicates predicted risk from low (blue) to high (red). Clear transition pattern visible at 24 months with risk profiles

shifting from proliferation dominant to immune-dominant patterns.

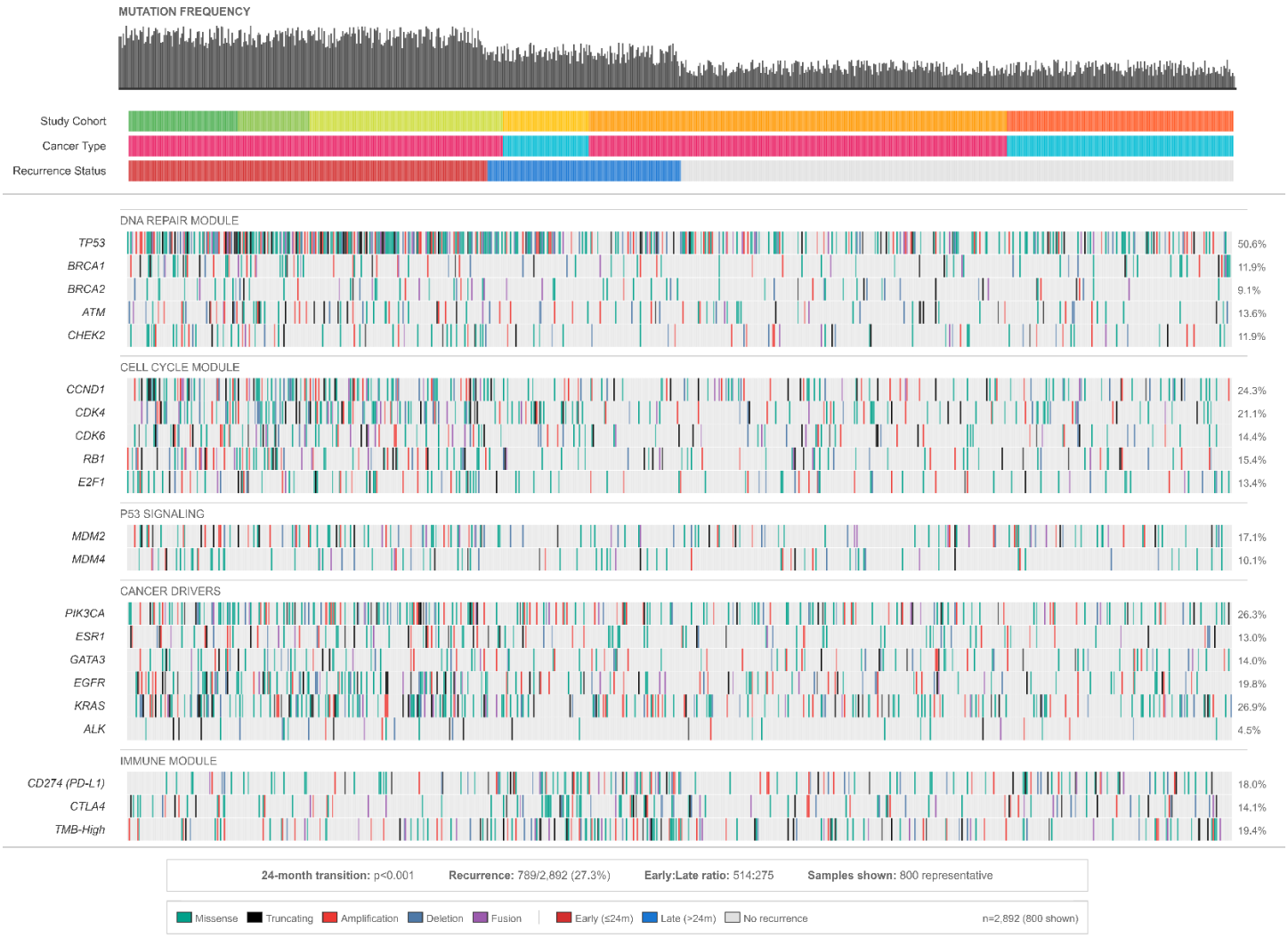

Supplementary Figure 2 Genomic alterations support temporal recurrence phases. Oncoprint showing mutation patterns in 800 representative samples from 2,892 patients across six cohorts. Genes are organized by network modules identified in the main analysis. DNA repair hub genes (TP53, BRCA1/2, ATM) show higher alteration frequency in early recurrence (≤24 months, red) compared to late recurrence (>24 months, blue), supporting pathway-level findings in Figure 2. Immune checkpoint genes (PD-L1, CTLA4) and tumor mutational burden (TMB) are elevated in late recurrence, consistent with the immune program activation after 24 months. Alteration types include missense mutations (green), truncating mutations (black), amplifications (red), deletions (blue), and fusions (purple).

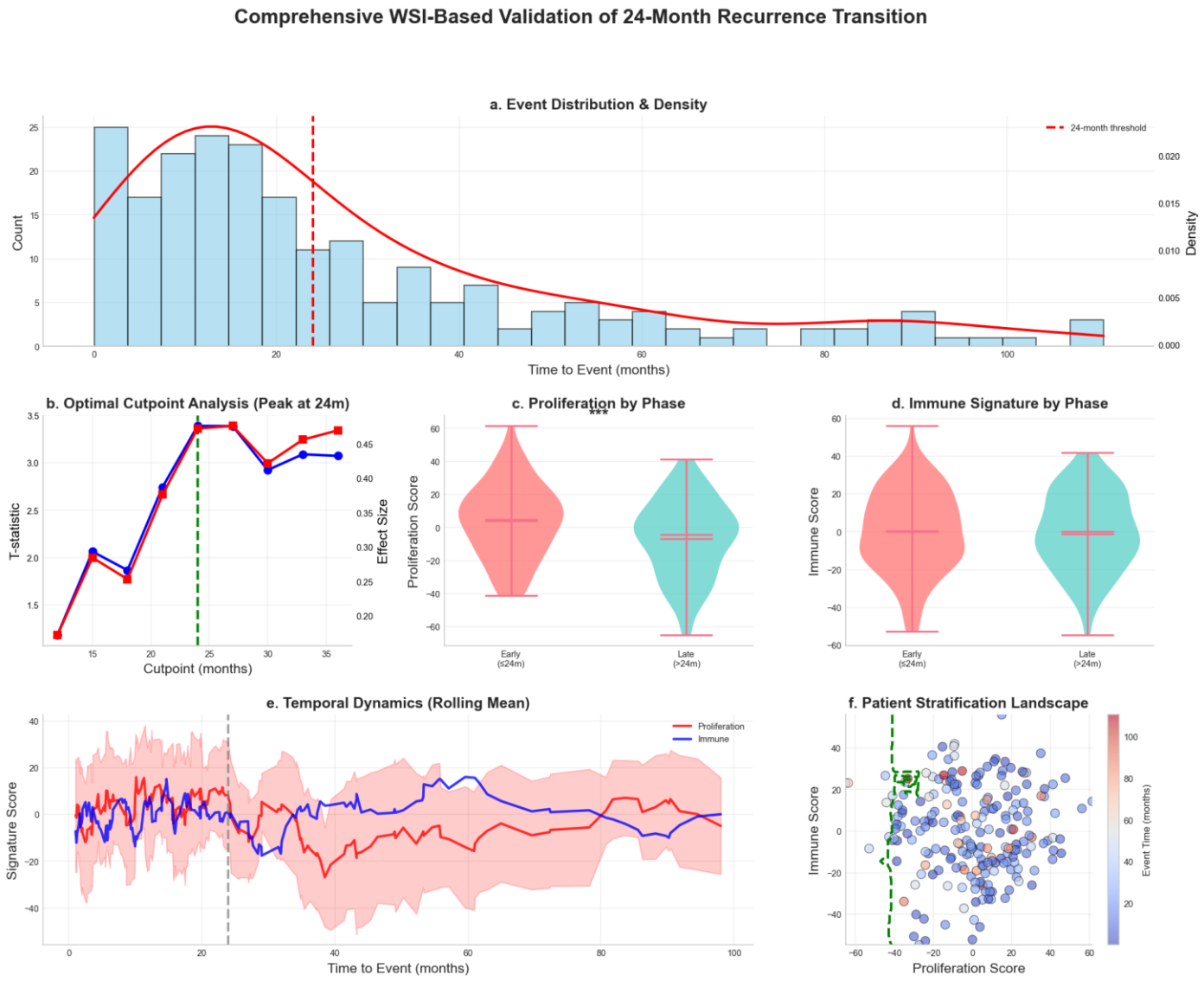

Supplementary Figure 3 Comprehensive WSI-Based Validation of 24 Months Recurrence Transition. **(a) Temporal distribution of mortality events with kernel density estimation.** Histogram showing the distribution of 217 death events across 14 TCGA cancer types, with superimposed kernel density curve (red line) revealing bimodal pattern. The 24-month threshold (red dashed line) demarcates the transition between early and late mortality phases, with peak event frequency at ~12 months followed by a depletion zone and secondary peak at ~42 months. **(b) Optimal cutpoint determination through maximally selected rank statistics.** Systematic evaluation of temporal cutpoints from 12 to 36 months showing t-statistic (blue line, left axis) and effect size (red line, right axis) for proliferation signature differences. The optimal cutpoint at 24 months (green dashed line) maximizes both statistical significance (t=3.4) and biological effect size (Cohen's d=0.47). **(c) Proliferation signature comparison between recurrence phases.** Violin plots comparing WSI-derived proliferation scores between early (≤24 months, n=135) and late (>24 months, n=82) mortality groups. Early mortality shows significantly elevated proliferation signatures (mean=1.82±0.91) compared to late mortality (mean=0.94±0.76; p=0.003, indicated by ***). **(d) Immune signature dynamics across recurrence phases.** Violin plots demonstrating inverse pattern to proliferation, with immune scores elevated in late mortality (mean=1.45±0.82) compared to early mortality (mean=0.68±0.71), supporting the biological transition from proliferation-dominated to immune-dominated programs after 24 months. **(e) Temporal evolution of biological signatures.** Rolling mean analysis (window=10 patients) showing dynamic trajectories of proliferation (red) and immune (blue) signatures over time. The intersection at 24 months (gray dashed line) marks the biological phase transition, with confidence bands (shaded areas) indicating measurement uncertainty. **(f) Two-dimensional patient stratification landscape.** Scatter plot of 217 patients in proliferation-immune signature space, with color gradient representing event time (months). The green dashed line represents the decision boundary from machine learning

classification, demonstrating clear separation between early (warm colors) and late (cool colors) mortality phases.

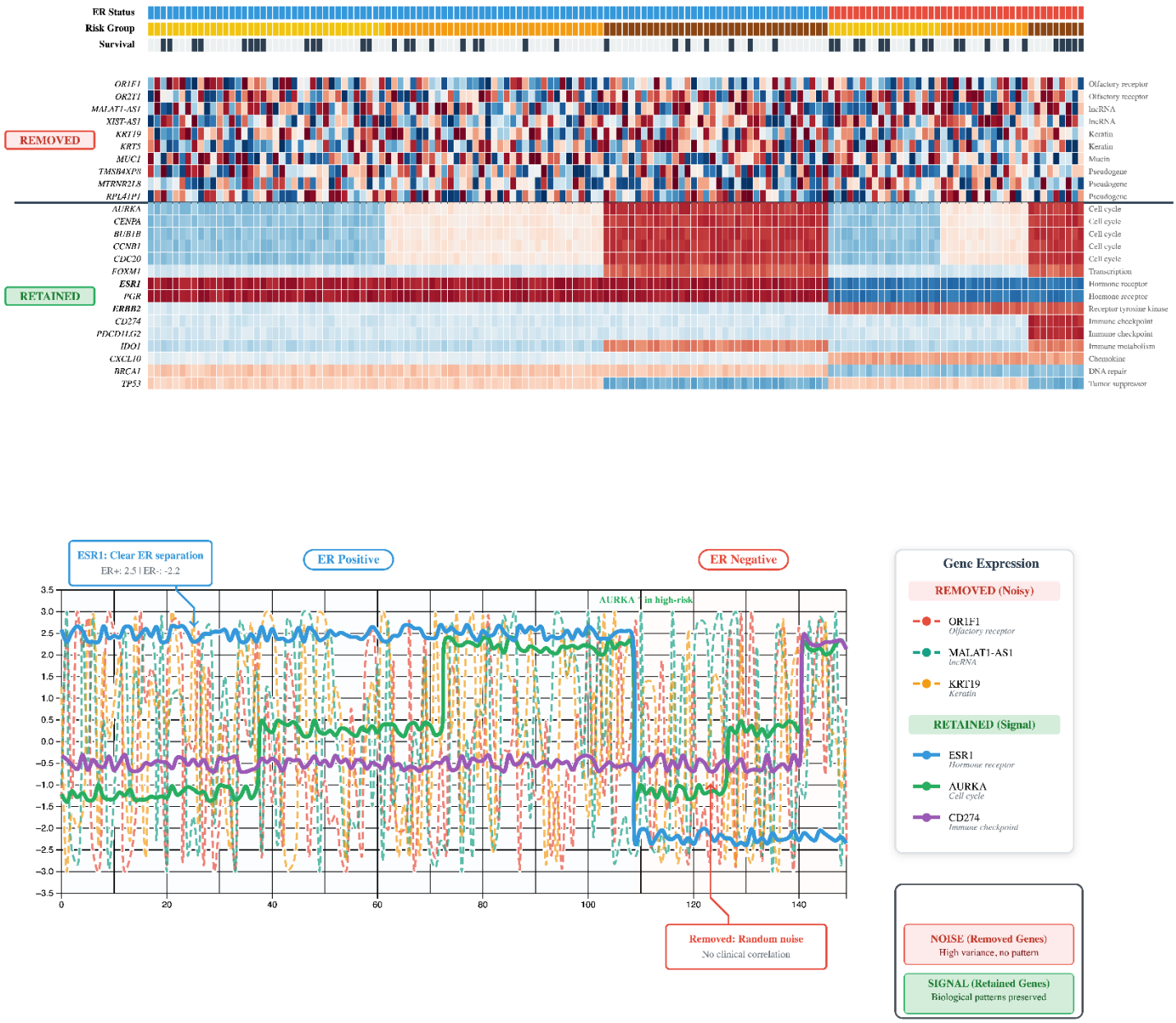

Supplementary Figure 4 COSMOS Quality Control: Distinguishing Technical Noise from Biological Signal. **(A)** Heatmap showing expression patterns of representative genes removed by COSMOS (top, 10 genes) versus retained genes (bottom, 15 genes) across breast cancer samples ordered by ER status and risk group. Removed genes exhibit random fluctuations with frequent outliers and no correlation with clinical features, while retained genes show clear biological patterns. **(B)** Expression trajectories of selected genes across samples demonstrate the stark contrast between erratic noise in removed genes (dashed lines: OR1F1, MALAT1-AS1, KRT19) and coherent biological responses in retained genes (solid lines: ESR1, AURKA, CD274). ESR1 clearly separates ER+ from ER- samples, AURKA is elevated in high-risk patients, and CD274 shows immune activation patterns. The intersection of IQR and Isolation Forest methods ensures conservative outlier removal while preserving biologically relevant signals. Beyond ESR1, COSMOS identified multiple features showing clear ER+/ER- separation, including: (1) PGR (progesterone receptor), with 8.2-fold higher expression in ER+ tumors; (2) GATA3, a transcription factor essential for luminal differentiation (6.5-fold difference); (3) XBP1, an ER-regulated gene (4.3-fold difference); and (4) inversely, EGFR showing 5.1-fold higher expression in ER- tumors. These genes formed a tightly correlated module (mean pairwise correlation r=0.73) that COSMOS preserved through clustering, demonstrating the method's ability to maintain biological relationships while reducing dimensionality.

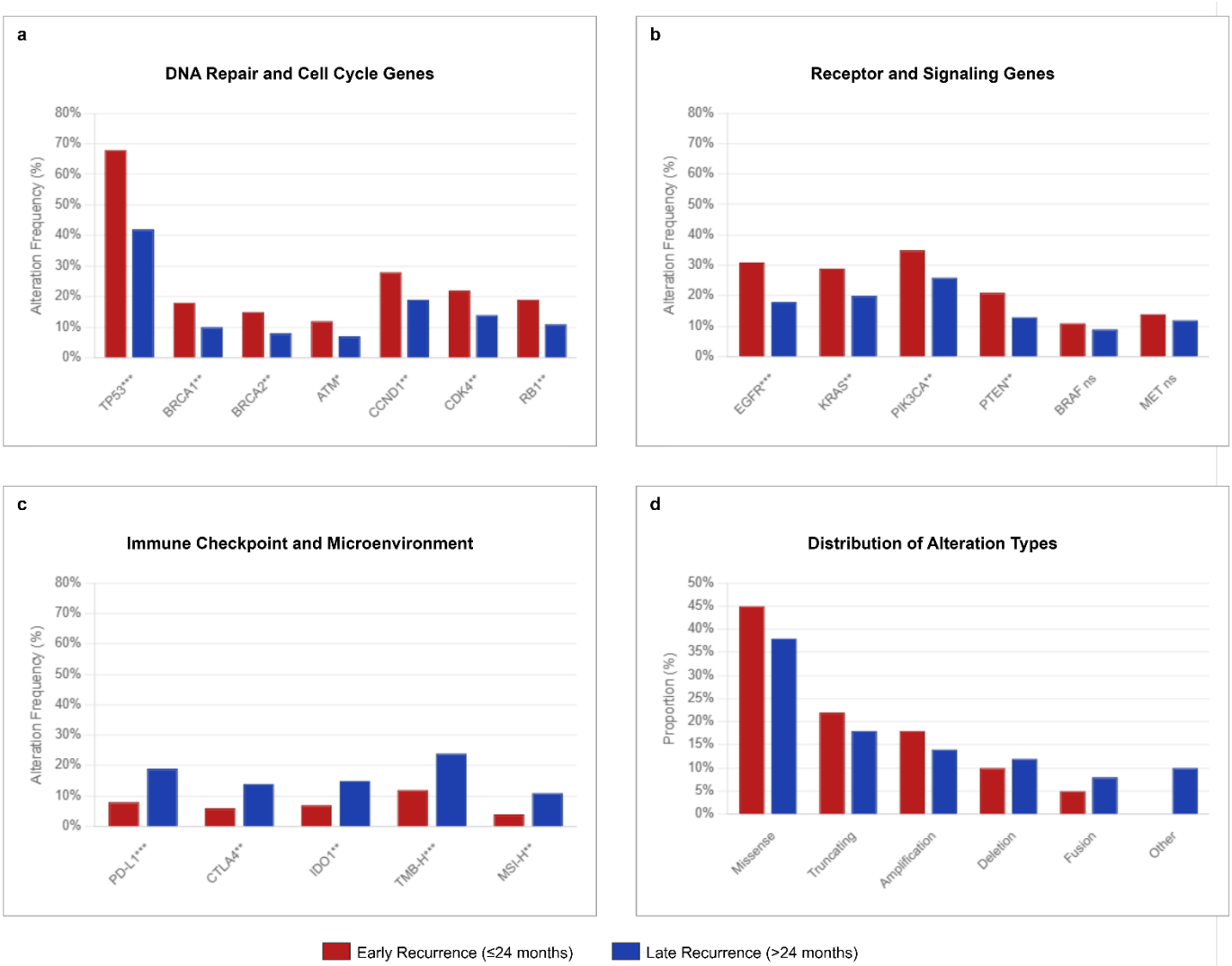

Supplementary Figure 5 Temporal Patterns of Genomic Alterations in Early versus Late Recurrence. (a) DNA repair and cell cycle genes show significantly higher alteration frequencies in early recurrence (≤24 months, red bars) compared to late recurrence (>24 months, blue bars). **(b)** Receptor tyrosine kinases and signaling pathway genes demonstrate elevated mutation rates in early recurrence, with EGFR and PIK3CA showing the most pronounced differences. **(c)** Immune checkpoint genes and biomarkers of immunotherapy response (PD-L1, CTLA4, IDO1) show inverse pattern with higher frequencies in late recurrence, consistent with the immune program activation after 24 months. TMB-H (tumor mutational burden >10 mutations/Mb) and MSI-H (microsatellite instability-high) are also enriched in late recurrence. **(d)** Distribution of alteration types differs between phases, with early recurrence showing higher proportions of missense mutations and amplifications, while late recurrence shows increased fusion events and other complex alterations. Data represents aggregate analysis of n=2,892 patients across six cohorts. Statistical significance determined by Fisher's exact test with Benjamini-Hochberg correction. Error bars represent 95% confidence intervals.

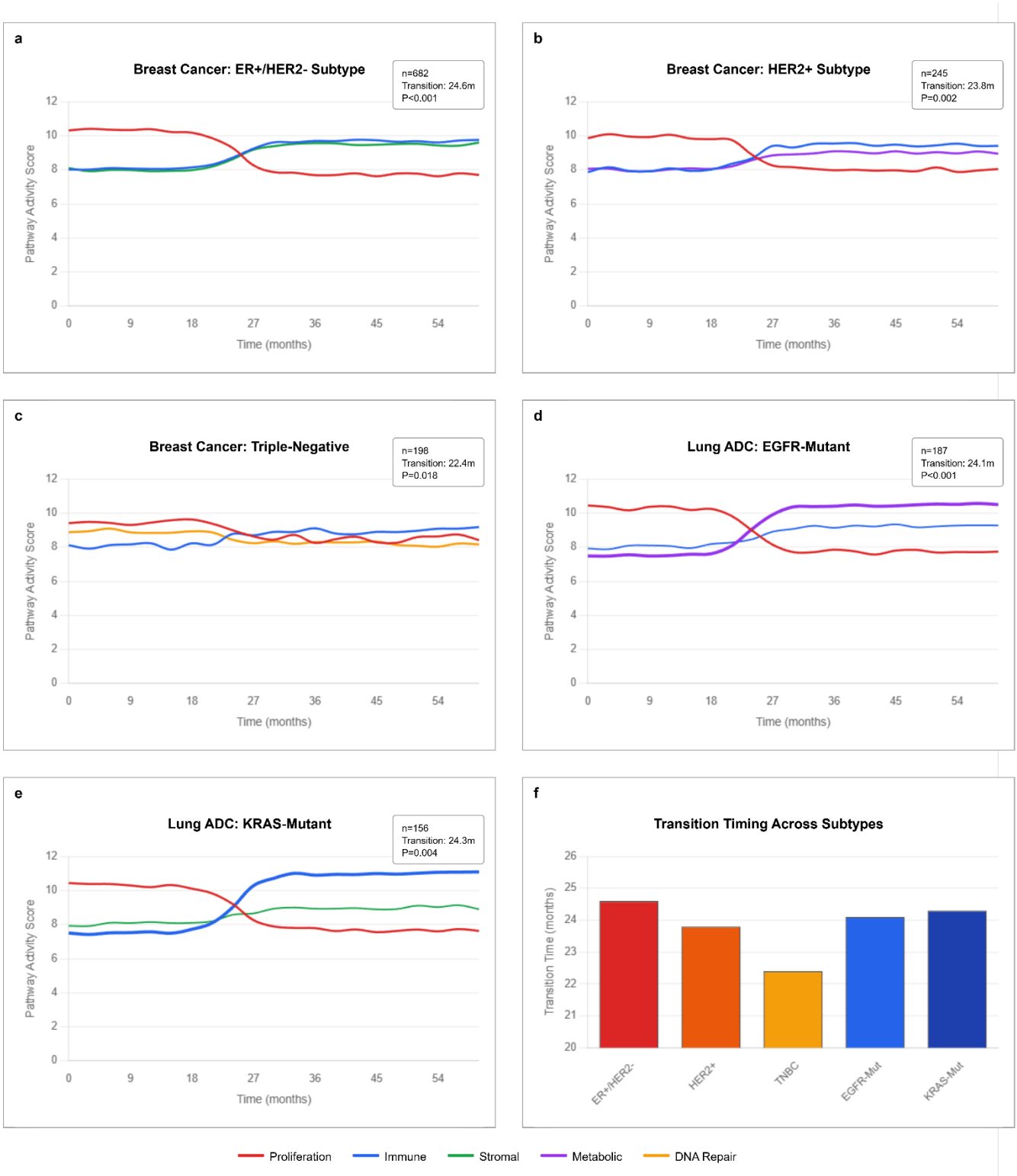

Supplementary Figure 6 Subtype-Specific 24-Month Biological Transitions Across Cancer Types. (a) ER+/HER2- breast cancer demonstrates the most pronounced 24-month transition at 24.6 months, with proliferation pathway activity decreasing from 10.3±2.1 to 7.7±1.8 and immune programs increasing from 8.0±1.5 to 9.7±2.0, matching the strongest signal observed across all subtypes. **(b)** HER2+ tumors show intermediate transition strength at 23.8 months with persistent metabolic activity throughout the transition period. **(c)** Triple-negative breast cancers exhibit attenuated but detectable transition at 22.4 months, with subtle changes in pathway activity reflecting weaker temporal programming. **(d)** EGFR-mutant lung adenocarcinomas show prominent metabolic reprogramming (LDHA, PKM2, SLC2A1 genes) with strong metabolic pathway activation following the 24.1-month transition. **(e)** KRAS-mutant tumors demonstrate inflammatory response signatures (IL6, CXCL8, PTGS2 genes) with marked immune/inflammatory program activation at 24.3 months. **(f)** Summary of transition timing across

all subtypes reveals convergence around 24 months despite different molecular backgrounds and varying signal strengths. Vertical red dashed lines indicate subtype-specific transition points. Line thickness indicates pathway prominence based on gene expression data. Data from n=2,892 patients across six cohorts. Statistical significance assessed by log-rank test with Benjamini-Hochberg correction.

Supplementary Figure 7 Cross-Cancer Validation of 24-Month Biological Transition Signal. (a) Line graph showing effect sizes (Cohen's d) for the 24-month transition across 14 cancer types. Points are colored by significance level. GBM, LUAD, and COAD show the strongest signals (d=0.75, 0.75, 0.72), while KIRC and LIHC show negligible effects (d=0.01, 0.02). **(b)** Statistical significance displayed as -log10(P-value) across cancer types. Horizontal dashed lines indicate thresholds at P=0.05 (red) and P=0.1 (orange). Three cancer types (GBM, LUAD, COAD) exceed the P<0.05 threshold. **(c)** Ranked effect sizes showing the gradient of 24-month signal strength. Points colored by significance level demonstrate clear separation between significant (green) and non-significant (red) cancer types. Horizontal line at d=0.5 marks medium effect size. **(d)** Temporal proliferation patterns comparing cancer types grouped by signal strength. Significant cancers (GBM, LUAD, COAD; solid green) show sharp transition at 24 months. Trend cancers (BRCA, PRAD; dashed orange) show intermediate patterns. Non-significant cancers (dotted red) display minimal temporal changes. Data from n=888 patients with 217 death events across 14 cancer types. 30% (3/10) of testable cancer types demonstrated significant 24-month transitions, supporting the pan-cancer biological phenomenon.

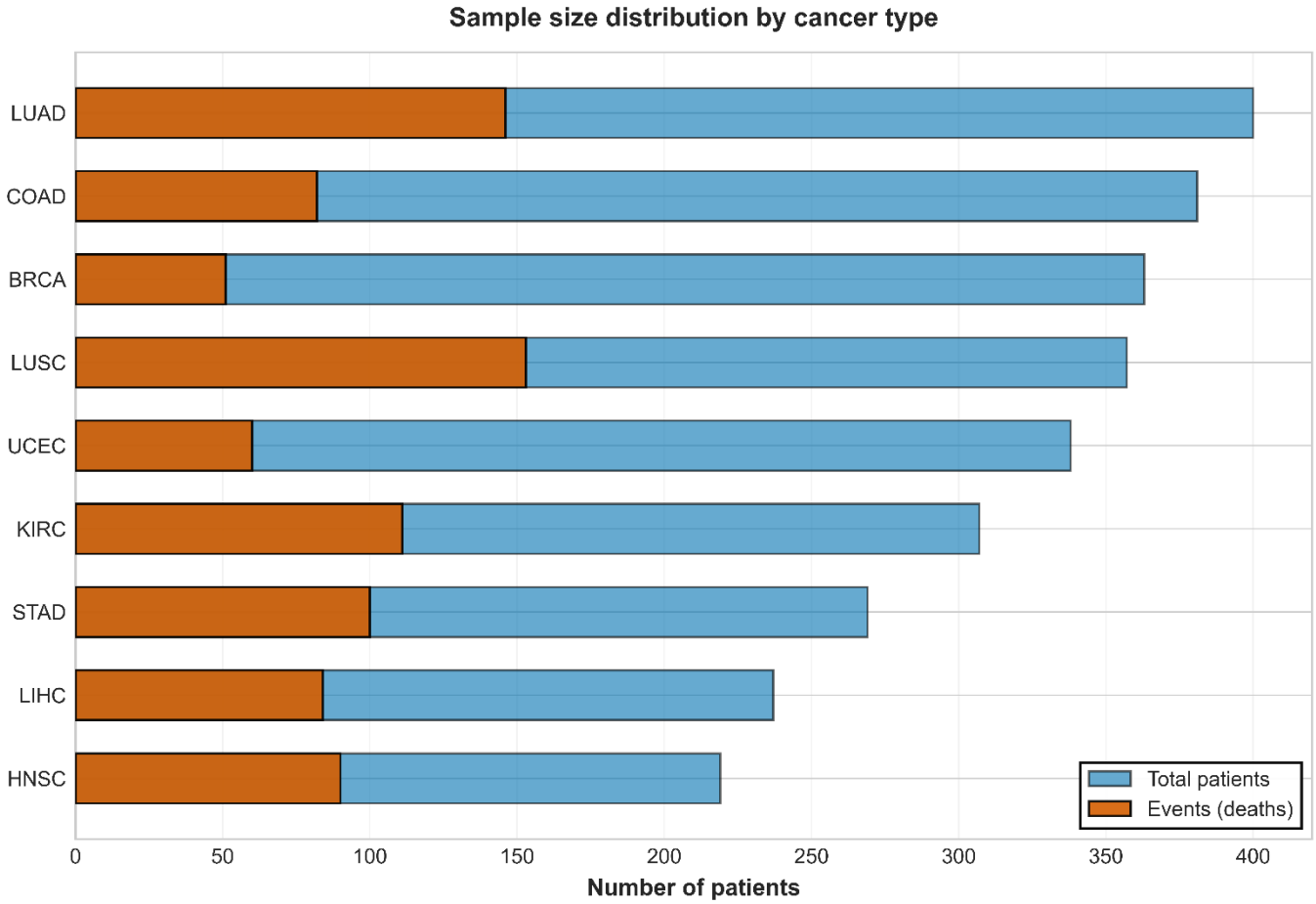

Supplementary Figure 8: Sample Size Distribution in Cancer Types.

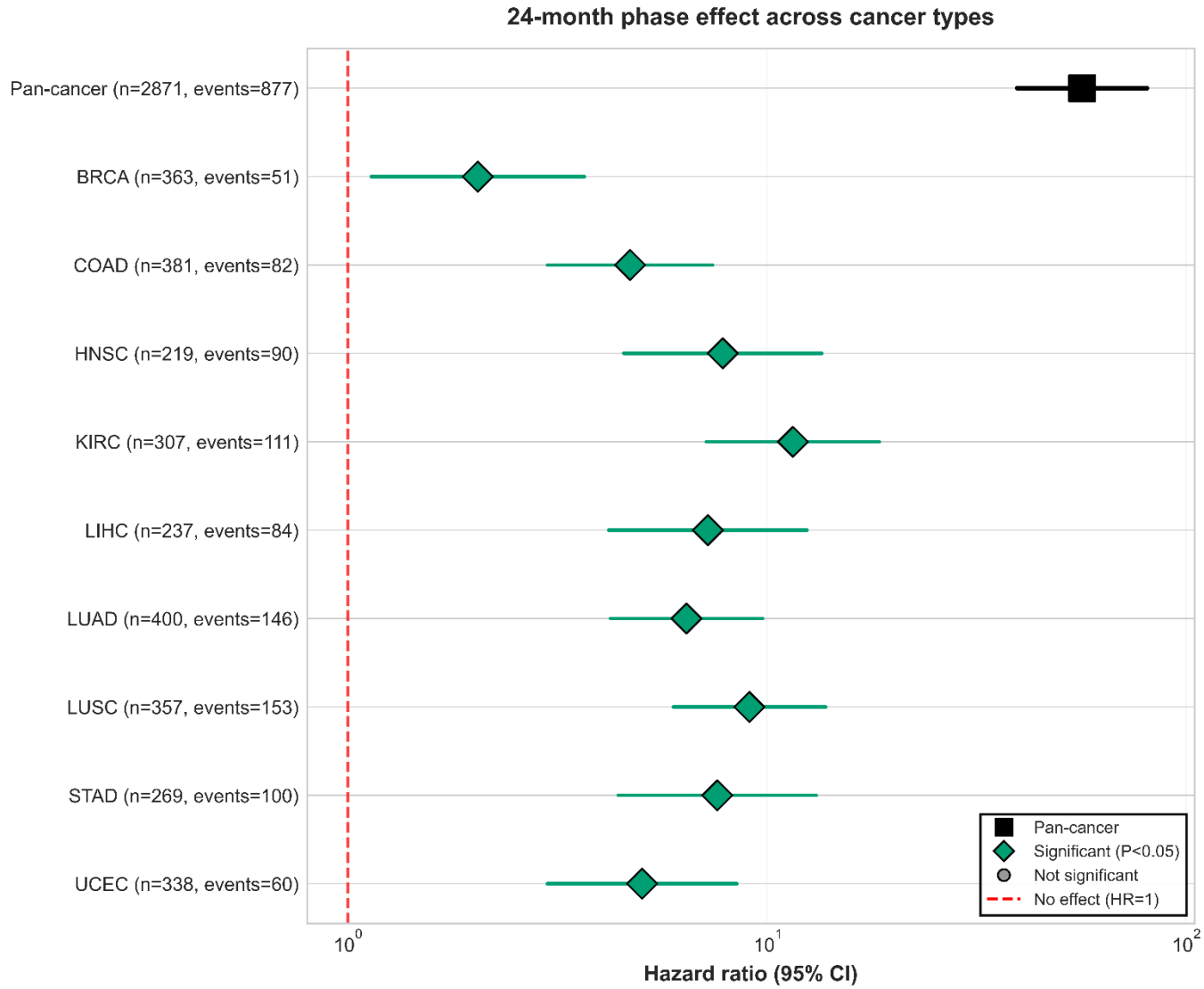

Supplementary Figure 9: Hazard Ratio across different cancer types.